

Barrier-Lowering Effects of Baird Antiaromaticity in Photoinduced Proton-Coupled Electron Transfer (PCET) Reactions

Lucas J. Karas,* Chia-Hua Wu, Judy I. Wu*

ABSTRACT: Baird antiaromaticity plays a central role in the photochemistry of proton-coupled electron transfer (PCET) reactions. We recognize that many popular organic chromophores that catalyze photoinduced PCET reactions are Hückel aromatic in the ground state, but gain significant Baird antiaromatic character in the lowest $\pi\pi^*$ state, having important barrier-lowering effects for electron transfer. Two examples, 1) the photolytic O–H bond dissociation of phenol and 2) solar water splitting in the pyridine-water complex, are discussed. Contrary to an assumed homolytic O–H bond dissociation, both reactions proceed through loss (and gain) of an electron in the π -system (i.e., antiaromaticity relief), followed by heterolytic cleavage of the polar O–H bond near barrierlessly. Nucleus-independent chemical shifts (NICS), ionization energies (IE), electron affinities (EA), and excited-state PCET energy profiles of selected $[4n]$ and $[4n+2]$ π -systems are presented.

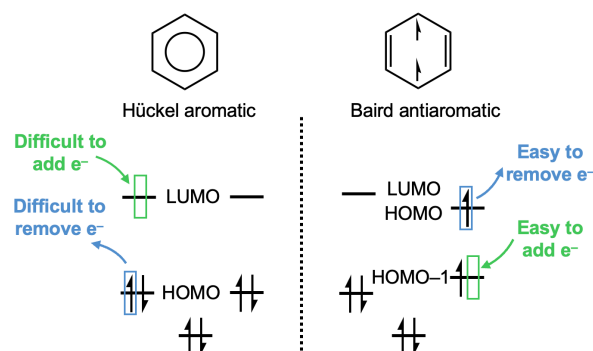
Photoinduced proton-coupled electron transfer (PCET) reactions are the critical steps to a myriad of energy conversion processes in organic photochemistry.^{1,2} In the case where an electron moves first, these reactions also can be called electron-driven proton transfer (EDPT)—an aromatic chromophore absorbs light, triggers the migration of an electron, and a proton follows. These reactions typically have low-barriers, and here, we make the connection between facile electron transfer and the concepts of ground and excited-state (anti)aromaticity. We note that the most common organic chromophores (e.g., phenol,³ pyridine,⁴ and other π -conjugated rings^{5,6}) are $[4n+2]$ Hückel aromatic in the ground state,⁷ but convert to $[4n+2]$ Baird antiaromatic in the lowest $\pi\pi^*$ state,⁸ and the high-energy π -system can easily lose (or gain) an electron triggering the first step of a photoinduced PCET reaction.

A representative example is the photolytic O–H bond fission of phenol. Flash photolysis and transient absorption studies of phenol in the vapor phase and in aqueous solution indicate the formation of neutral phenoxy radicals.^{9,10} According to *ab initio* studies and kinetic experiments, UV irradiation first generates an optically active $\pi\pi^*$ state, then O–H σ -bond fission resolves in a dark $\pi\sigma^*$ state, reached by nonadiabatic interaction of the two surfaces.^{5,11–13} It was reported for many other aromatic chromophores, that photolytic O–H or N–H bond fission proceeded through similar dissociative charge transfer states.^{3,6,14} The net outcome of these reactions is σ -bond cleavage, but it is the π -ring that absorbs light.

Traditionally, the driving force for photoinduced electron transfer has been explained by the Rehm-Weller model,¹⁵ where Gibbs free energy for charge separation is estimated by the oxidation and reduction potential of the electron donor and acceptor, respectively. But here, we show that a more complete picture emerges when the effects of excited-state (anti)aromaticity are considered. A number of works have recognized the role of excited-state antiaromaticity in organic photoreactions (e.g., the photoionization of haloaromatic compounds,¹⁶ phototriggered bond breaking,^{17,18}

photodeactivation of DNA base pairs,¹⁹ photoreaction of benzene,²⁰ and excited-state proton transfer^{21,22}).

In this paper, we demonstrate that Hückel aromatic chromophores can gain significant Baird antiaromatic character in the lowest $\pi\pi^*$ states, and the emergence of excited-state antiaromaticity catalyzes electron transfer. Our arguments are developed first based on a comparison of energy profile of the photoinduced PCET reactions of phenol, hydroxyl-cyclooctatetraene, and derivatives of these model systems in the T_1 state, followed by a detailed theoretical analysis of two photoinduced PCET reactions in the S_1 state: 1) the photolytic bond fission of phenol, and 2) solar water splitting from a pyridine-water complex.



Scheme 1. Schematic illustration of frontier molecular orbitals of benzene in the S_0 (aromatic) and T_1 (antiaromatic) states.

Consider the frontier molecular orbital energies of benzene (Scheme 1). In the S_0 state, benzene is Hückel aromatic, there is a large orbital splitting between the degenerate set of highest occupied molecular orbitals (HOMO) and lowest unoccupied molecular orbitals (LUMO), and both removing an electron from the low-lying HOMO and adding an electron to the high-lying LUMO are energetically costly (Scheme 1, left). But in the T_1 ($^3\pi\pi^*$) state, benzene

is Baird antiaromatic and this is characterized by a small orbital splitting (i.e., Jahn-Teller distortion of the degenerate set of antibonding π -orbitals).²³⁻²⁶ Now the HOMO is a half-filled orbital belonging to a degenerate set of antibonding orbitals, and removing an electron from this high-lying orbital becomes easier. The HOMO-1, a low-lying bonding orbital, also readily accepts an electron (Scheme 1, right). In this way, aromaticity and antiaromaticity can be linked to the ease of removing or adding an electron to a π -system.

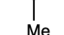
Computed ionization energies (IE) and electron affinities (EA) for toluene and methylenecyclohexadiene in the S_0 and T_1 states are illustrative. In the S_0 state, toluene is $[4n+2]$ Hückel aromatic (NICS(1)_{zz} = -26.5 ppm) and exhibits both a higher IE (+8.8 eV) and a higher EA (+2.1 eV) compared to the nonaromatic isomer (IE = +7.7 eV, EA = +0.7 eV) (Figure 1a, left). But in the T_1 state, toluene is $[4n+2]$ Baird antiaromatic (NICS(1)_{zz} = +38.7 ppm) and displays both a lower IE (+5.3 eV) and a lower EA (-2.0 eV) compared to the T_1 state of the nonaromatic isomer (IE = +6.1 eV, EA = -1.0 eV) (Figure 1a, right). Nucleus-independent chemical shifts, NICS(1)_{zz}, were computed at 1 Å above the ring centers including only the out-of-plane (zz) tensor component.²⁷⁻²⁹ Negative NICS(1)_{zz} values indicate aromaticity and positive NICS(1)_{zz} values indicate antiaromaticity.

Computed IE and EA data for the S_0 and T_1 states of planar $[4n]$ methyl-cyclooctatetraene (COT) and planar methylenecyclooctatriene show the opposite trend. Planar methyl-COT is $[4n]$ Hückel antiaromatic (NICS(1)_{zz} = +35.5 ppm), and exhibits both a lower IE (+7.2 eV) and a lower EA (-0.7 eV) compared to the nonaromatic isomer (IE = +7.7 eV, EA = +0.1 eV) (Figure 1b, left). But in the T_1 state, methyl-COT is $[4n]$ Baird aromatic (NICS(1)_{zz} = -24.1 ppm) and displays a higher IE (+6.8 eV) and a higher EA (-1.0 eV) compared to that of the nonaromatic isomer (IE = +6.1 eV, EA = -1.5 eV) (Figure 1b, right). Zhu and Schleyer have shown that isomerization energies of the S_0 and T_1 states of such pairs provide reliable energetic measures for ground and triplet state (anti)aromaticity.³⁰ All geometries were optimized with a constrained C_s symmetry, and energies were computed at CASPT2/6-311+G(d,p)//CASSCF/6-311+G(d,p) using Molpro 2012.³¹ NICS(1)_{zz} for six-membered ring systems were computed at CASSCF/6-311+G(d,p), and for eight-membered ring systems, at CASSCF/6-31G(d,p), using the Dalton2016 program.^{32,33}

Figure 2 compares the T_1 state PCET energy profiles of 4-methyl-phenol (**1**, $[4n+2]$) and 1-hydroxy-5-methyl-COT (**2**, $[4n]$) with that of their nonaromatic isomers (**1'** and **2'**). Potential energy profiles along the O-H stretching coordinate were computed at 0.1 Å intervals in the $^3\pi\pi^*$ and $^3\pi\sigma^*$ states (see Figure S4 for the S_1 state results). As the O-H bond stretches, the $^3\pi\pi^*$ and $^3\pi\sigma^*$ curves intersect and crossing of the two functions marks the point at which an electron transfers from the π -ring to the acidic H atom. Barriers to electron transfer (ΔE_{ET}) were estimated based on the energy measured at the crossing of the interpolated $^3\pi\pi^*$ and $^3\pi\sigma^*$ curves minus the energy of the $^3\pi\pi^*$ at O-H = 1 Å. **1** (Baird antiaromatic) displays a high T_1 state energy (80.7 kcal/mol) and the $^3\pi\pi^*$ to $^3\pi\sigma^*$ intersection occurs "early" through a relatively low barrier (ΔE_{ET} = 27.3 kcal/mol, at O-H = 1.26 Å) (Figure 2a, left). In contrast, **1'** (nonaromatic) exhibits a lower T_1 state energy (38.3 kcal/mol) and the conical intersection occurs "late" through a nearly doubled barrier (ΔE_{ET}

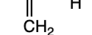
= 57.0 kcal/mol, at O-H = 1.47 Å) (Figure 2b, left). Computed NICS(1)_{zz} values for **1**, at geometries along the photoinduced PCET pathway, show an abrupt drop in paratropicity past the $^3\pi\pi^*$ to $^3\pi\sigma^*$ intersection (Figure 2a, right, note the sign change of NICS(1)_{zz} values from positive to negative), while those of **1'** remain constant for both the $^3\pi\pi^*$ and $^3\pi\sigma^*$ states, having values close to zero (Figure 3b, right). We recognized the high T_1 state energy of **1** as a consequence of Baird antiaromaticity, and facile electron transfer is the escape from it.

a)



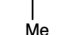
Me

Hückel aromatic

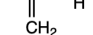


CH₂

Baird antiaromatic




Me



CH₂

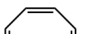
IE (eV)	+8.8	+7.7	+5.3	+6.1
EA (eV)	+2.1	+0.7	−2.0	−1.0
NICS(1) _{zz} (ppm)	−26.5	+5.8	+38.7	+0.3

b)




Me

Hückel antiaromatic

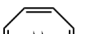


CH₂

Baird aromatic



Me



CH₂

IE (eV)	+7.2	+7.7	+6.8	+6.1
EA (eV)	−0.7	+0.1	−1.0	−1.5
NICS(1) _{zz} (ppm)	+35.5	+1.8	−24.1	+7.1

Figure 1. Computed ionization energies (IE), electron affinities (EA), and NICS(1)_{zz} values of a) toluene vs. methylenecyclohexadiene, and b) planar methyl-COT vs. methylenecyclooctatriene, in the S_0 and T_1 states.

Potential energy profiles for the triplet states of **2** vs. **2'** show the opposite trend. **2** (Baird aromatic) exhibits a low T_1 state energy (5.9 kcal/mol) and crossing from the $^3\pi\pi^*$ state to the $^3\pi\sigma^*$ state involves a high barrier (ΔE_{ET} = 69.5 kcal/mol, at O-H = 1.56 Å) due to a largely stabilized T_1 state (Figure 2c, left). In comparison, **2'** (nonaromatic) has a higher T_1 state energy (31.5 kcal/mol) and a lower barrier to electron transfer (ΔE_{ET} = 56.5 kcal/mol, at O-H = 1.47 Å) (Figure 2d, left, note the similar T_1 energies and ΔE_{ET} values compared to **1'**, cf. Figure 2b). Computed NICS(1)_{zz} values at geometries along the photoinduced PCET pathway of **2** show a sudden raise in paratropicity past the $^3\pi\pi^*$ to $^3\pi\sigma^*$ intersection (Figure 3c, right, note the sign change of NICS(1)_{zz} values from negative to positive), while those of **2'** remain relatively constant for both the $^3\pi\pi^*$ and $^3\pi\sigma^*$ states (Figure 2d, right). Computed gauge-including magnetically induced current (GIMIC)³⁴ plots, ¹H chemical shifts, and harmonic oscillator model of aromaticity (rHOMA)³⁵ agree with NICS see data in the Supporting Information, SI).

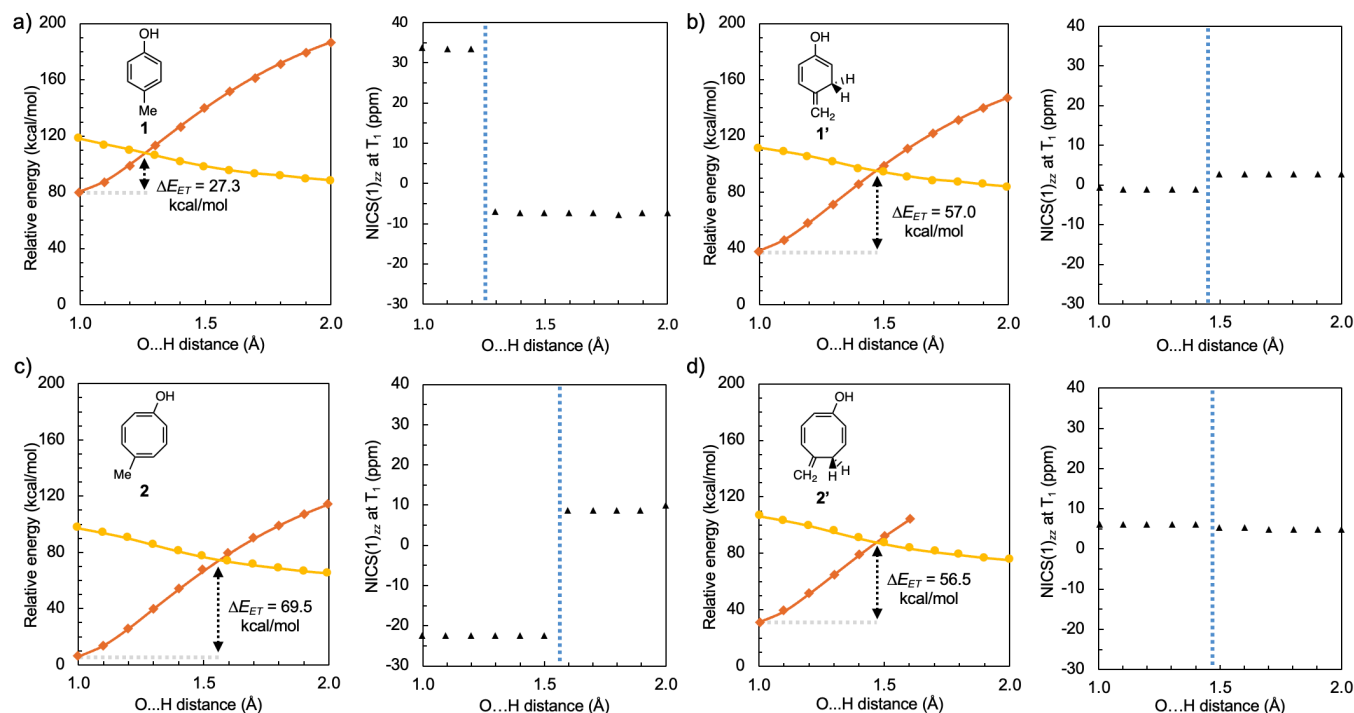


Figure 2. Computed potential energy profiles (in kcal/mol) along the O–H stretching coordinate at 0.1 Å intervals in the $^3\pi\pi^*$ (orange rhomboids) and $^3\pi\sigma^*$ (yellow circles) states for a) **1**, b) **1'**, c) **2**, and d) **2'**, and NICS($1)_{zz}$ values (in ppm) computed along the photoinduced PCET pathway crossing the LE and CT states. In the NICS plots, the vertical blue dotted lines indicate crossing of the LE and CT states. All energies are relative to the S_0 state energy at O–H = 1.0 Å.

Barrier-lowering effects of Baird antiaromaticity for photoinduced PCET reactions extend also to the S_1 state,^{36–39} in which reactions such as the photolysis of phenol take place. In the lowest $^1\pi\pi^*$ state, phenol displays a low barrier to PCET ($\Delta E_{ET} = 20.7$ kcal/mol, at O–H = 1.21 Å, Figure 3a) and computed NICS($1)_{zz}$ values at geometries along the photoinduced PCET pathway show decreased paratropicity immediately past the intersection of the locally excited (LE) $^1\pi\pi^*$ state and charge transfer (CT) $^1\pi\sigma^*$ state (Figure 3b, see Figure S5 for the T_1 results). The importance of the $^1\pi\sigma^*$ CT state has been recognized in earlier theoretical and experimental works,^{5,11} but here, we emphasize the mechanistic implications of this electron transfer step.

As shown in Figure 3c, the photolytic O–H bond dissociation of phenol must happen *heterolytically* to give homolytic products (Figure 3c, bottom). Because the end products of the reaction are H^\bullet and a phenoxy radical (PhO^\bullet), it is tempting for the trained organic chemist to illustrate bond dissociation by two sets of single-headed arrows showing homolytic cleavage of the OH σ -bond (Figure 3c, top). But the reaction cannot happen this way. The > 80 kcal/mol homolytic O–H bond dissociation energy is much too high (note the parallel displaced S_0 and $^1\pi\pi^*$ state curves)! Heterolytic cleavage of the polar O–H bond requires much less energy (i.e., both electrons move towards the more electronegative O atom) and occurs readily upon crossing of the $\pi\pi^*$ and $\pi\sigma^*$ states. At the conical intersection, an electron moves away from the π -ring and the CT state ($^1\pi\sigma^*$) is stabilized as the proton follows, giving the radical products. We note that closely related reactions such as the photo-Fries rearrangement of phenyl esters, also are commonly illustrated

in Google searches and textbooks as homolytic O–R bond cleavage processes and suggest that the arrow pushing mechanisms of these reactions also ought to be redrawn.^{40,41}

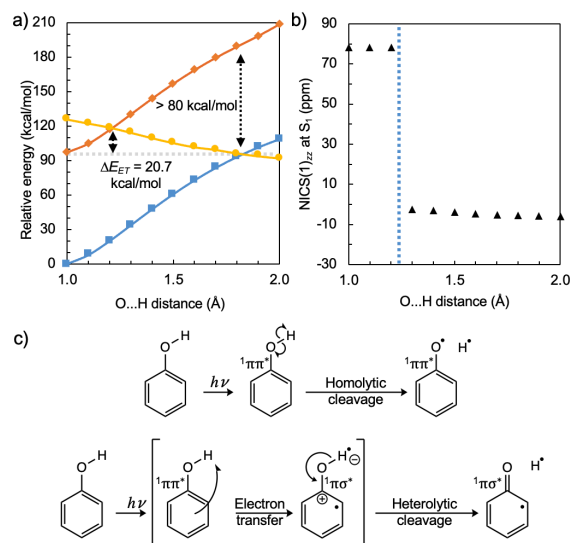


Figure 3. a) Computed potential energy profiles (in kcal/mol) along the O–H stretching coordinate at 0.1 Å intervals, in the S_0 (blue squares), LE ($^1\pi\pi^*$, orange rhomboids), and CT ($^1\pi\sigma^*$, yellow circles) states for phenol, and b) NICS($1)_{zz}$ values (in ppm) computed along the photoinduced PCET pathway crossing the LE and CT states. All energies are relative to the S_0 state energy at O–H = 1 Å. c) Photoinduced homolytic vs. heterolytic O–H bond breaking mechanisms.

We further considered the phototriggered water splitting reaction of a model pyridine (Py)-water complex. Photodeactivation through PCET was suggested as a reason for the absence of fluorescence of pyridine in water.^{4,42-46} Water splitting through this route requires two photons. In the first step, pyridine absorbs light ($\pi\pi^*$, LE state), and an electron moves from water to the photoexcited π -ring followed by proton transfer ($\pi\pi^*$ or $n\pi^*$, CT state), generating a PyH^\bullet and OH^\bullet radical pair. The triplet CT state is degenerate with the singlet state and can be reached through efficient intersystem crossing. Photoreactions on the excited singlet and triplet state surfaces were shown to be quite similar. In the next step, a second photon detaches H^\bullet from PyH^\bullet and regenerates the catalytic pyridine. Without the chromophore, homolytic bond cleavage of an O–H bond in water (in the gas phase) is 5.1 eV.⁴⁷ Here, we examine the first step of the reaction, showing that in the lowest $\pi\pi^*$ state the catalytic pyridine ring is Baird antiaromatic, and that adding an electron from water to the pyridine ring alleviates excited-state antiaromaticity.

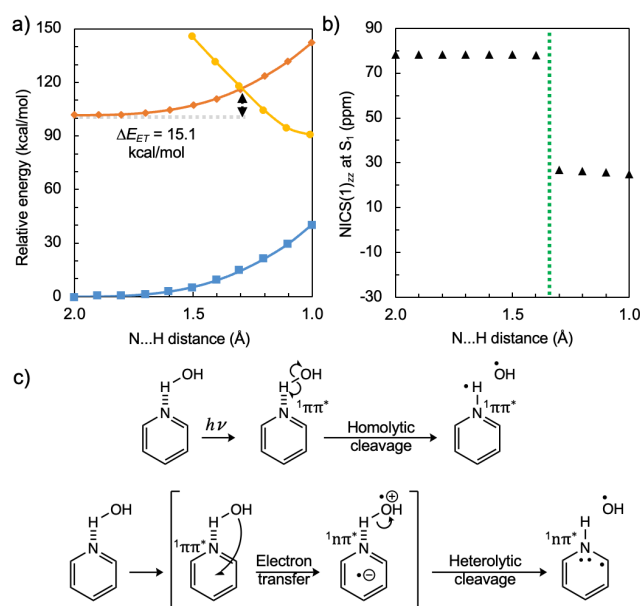


Figure 4. a) Computed potential energy profiles (in kcal/mol) along the N–H bond forming coordinate at 0.1 Å intervals, in the S₀ (blue squares), LE (¹ππ*, orange rhomboids), and CT (¹nπ*, yellow circles) states for the (Py)-water complex, and b) NICS(1)_{zz} values (in ppm) computed along the photoinduced PCET pathway crossing the LE and CT states. All energies are relative to the S₀ state energy at O–H = 1 Å. c) Photoinduced homolytic vs. heterolytic O–H bond breaking mechanisms.

Figure 4a shows the computed energy profiles of the (Py)-water complex at 0.1 Å intervals along the N–H bond forming coordinate (i.e., H moving from water to the pyridinyl N) in the S₀ state, LE state (¹ππ*), and CT state (¹nπ*, i.e., electron transfer from the hybridized lone pair of O to the pyridinyl ring). It was shown that crossing from the ¹ππ* LE state to the ¹nπ* CT state (i.e., electron transfer from the unhybridized lone pair of O to the pyridinyl ring) produced a similar energetic profile.⁴ As the N–H bond forms, the LE and CT curves intersect and crossing of the two functions marks

the point at which an electron transfers from water to the π -ring, and the water O–H bond breaks heterolytically (Figure 4c). Note the low barrier to PCET ($\Delta E_{ET} = 15.1$ kcal/mol, at N–H = 1.29 Å cf. 5.1 eV homolytic bond dissociation). Computed NICS(1)_{zz} values at geometries along the reaction pathway show a drop in paratropicity past the LE and CT state intersection (Figure 4b, see Figure S6 for the T₁ results).

Even though all photoexcited molecules can be thought to be “unstable,” the strong π -destabilizing effect of Baird antiaromaticity makes it a tremendously useful concept for designing photocatalytic chromophores and electron transfer reactions. We hypothesize that the highly positive excited-state reduction potentials of popular organic photoredox catalysts (e.g., acridine and acridium catalysts, 14 ring π -electrons)⁴⁸⁻⁵³ may be in part attributed to Baird antiaromaticity.

ASSOCIATED CONTENT

Supporting Information

The Supporting Information is available free of charge on the ACS Publications website.

Optimized Cartesian coordinates, computed ¹H chemical shifts, rHOMA analyses, GIMIC plots, as well as NICS(1)_{zz} and PCET energy profiles of **1** and **1'** in the S₁ state, and phenol and (Py)-water in the T₁ state are included along with a full methods section.

AUTHOR INFORMATION

Corresponding Author

Judy I. Wu – Department of Chemistry, University of Houston, Houston, Texas 77204, United States; orcid.org/0000-0003-0590-5290; Email: jiwu@central.uh.edu

Lucas J. Karas – Department of Chemistry, University of Houston, Houston, Texas 77204, United States; orcid.org/0000-0001-7970-119X; Email: lucaskaras@gmail.com

Authors

Chia-Hua Wu – Department of Chemistry, University of Houston, Houston, Texas 77204, United States; orcid.org/0000-0001-6850-3024

ACKNOWLEDGMENT

JIW thanks the National Science Foundation (CHE-1751370), the National Institute of General Medical Sciences of the National Institute of Health (R35GM133548), and the Alfred P. Sloan Research Foundation (FG-2020-12811) for support. We acknowledge the use of the Sabine cluster and support from the Research Computing Data Core at the University of Houston. Particularly, we thank Professor Henrik Ottosson for helpful suggestions for improving the manuscript.

REFERENCES

- (1) Weinberg, D. R.; Gagliardi, C. J.; Hull, J. F.; Murphy, C. F.; Kent, C. A.; Westlake, B. C.; Paul, A.; Ess, D. H.; McCafferty, D. G.; Meyer, T. J. Proton-coupled electron transfer. *Chem. Rev.* **2012**, *112*, 4016–4093.
- (2) Gagliardi, C. J.; Westlake, B. C.; Kent, C. A.; Paul, J. J.; Papanikolas, J. M.; Meyer, T. J. Integrating proton coupled electron transfer (PCET) and excited states. *Coord. Chem. Rev.* **2010**, *254*, 2459–2471.

- (3) Domcke, W.; Sobolewski, A. L. Unraveling the molecular mechanism of photoacidity. *Science*, **2003**, 302, 1693–1694.
- (4) Liu, X.; Sobolewski, A. J.; Borrelli, R.; Domcke, W. Computational investigation of the photoinduced homolytic dissociation of water in the pyridine-water complex. *Phys. Chem. Chem. Phys.* **2013**, 15, S957–S966.
- (5) Ashfold, M. N. R.; Cronin, B.; Devine, A. L.; Dixon, R. N.; Nix, M. G. D. The role of $\pi\sigma^*$ excited states in the photodissociation of heteroaromatic molecules. *Science*, **2006**, 312, 1637–1640.
- (6) Sobolewski, A. L.; Domcke, W. Computational studies of the photo-physics of hydrogen-bonded molecular systems. *J. Phys. Chem. A* **2007**, 111, 11725–11735.
- (7) Hückel, E. Z. Quantentheoretische beiträge zum benzolproblem. *1932*, 70, 204–286.
- (8) Baird, N. C. Quantum organic photochemistry: II. Resonance and aromaticity in the lowest $^3\pi\pi^*$ state of cyclic hydrocarbons. *J. Am. Chem. Soc.* **1972**, 94, 4941–4948.
- (9) Land, E. J.; Porter, G. Primary photochemical processes in aromatic molecules. Part. 7.—spectra and kinetics of some phenoxyl derivatives. *Trans. Faraday Soc.*, **1963**, 59, 2016–2026.
- (10) G. Dobson, L. I. Grossweiner. Flash photolysis of aqueous phenol and cresols. *Trans. Faraday Soc.*, **1965**, 61, 708–714.
- (11) Sobolewski, A. L.; Domcke, W. Photoinduced electron and proton transfer in phenol and its clusters with water and ammonia. *J. Phys. Chem. A* **2001**, 105, 9275–9283.
- (12) Sobolewski, A. L.; Domcke, W.; Dedoner-Lardeux, C.; Juvet, C. Excited-state hydrogen detachment and hydrogen transfer driven by repulsive $^1\pi\sigma^*$ states: a new paradigm for nonradiative decay in aromatic biomolecules. *Phys. Chem. Chem. Phys.* **2002**, 4, 1093–1100.
- (13) Nix, M. G. D.; Devine, A. L.; Cronin, B.; Dixon, R. N. Ashfold, M. N. R. High resolution photofragment translational spectroscopy studies of the near ultraviolet photolysis of phenol. *J. Chem. Phys.* **2006**, 125, 133318.
- (14) Ashfold, M. N. R.; King, G. A.; Murdock, D.; Nix, M. G. D.; Oliver, T. A. A.; Sage, A. G. $\pi\sigma^*$ excited states in molecular photochemistry. *Phys. Chem. Chem. Phys.* **2010**, 12, 1218–1238.
- (15) Rehm, D.; Weller, A. Kinetics of fluorescence quenching by electron and H-atom transfer. *Isr. J. Chem.* **1970**, 8, 259–271.
- (16) Jorner, K.; Rabten, W.; Slanina, T.; Vedin, N. P.; Sillén, Ludvigsson, J. W.; Ottosson, H.; Norrby, P.-O. Degradation of pharmaceuticals through sequential photon absorption and photoionization in amiloride derivatives. *Cell Rep. Phys. Sci.* **2020**, 1, 100274.
- (17) Halder, D.; Paul, A. Understanding the role of aromaticity and conformational changes in bond dissociation processes of photo-protecting groups. *J. Phys. Chem. A* **2020**, 124, 3976–3983.
- (18) Banerjee, A.; Halder, D.; Ganguly, G.; Paul, A. Deciphering the cryptic role of a catalytic electron in a photochemical bond dissociation using excited state aromaticity markers. *Phys. Chem. Chem. Phys.* **2016**, 18, 25308–25314.
- (19) Karas, L. J.; Wu, C.-H.; Ottosson, H.; Wu, J. I. Electron-driven proton transfer relieves excited-state antiaromaticity in photoexcited DNA base pairs. *Chem. Sci.* **2020**, 11, 10071–10077.
- (20) Slanina, T.; Ayub, R.; Toldo, J.; Sundell, J.; Rabten, W.; Nicaso, M.; Alabugin, I.; Galván, I. F.; Gupta, A. K.; Lindh, R.; Orthaber, A.; Lewis, R. J.; Grönberg, G.; Bergman, J.; Ottosson, H. Impact of excited-state antiaromaticity relief in a fundamental benzene photoreaction leading to substituted bicyclo[3.1.0]hexenes. *J. Am. Chem. Soc.* **2020**, 142, 10942–10954.
- (21) Wu, C.-H.; Karas, L. J.; Ottosson, H.; Wu, J. I. Excited-state proton transfer relieves antiaromaticity in molecules. *Proc. Natl. Acad. Sci. USA* **2019**, 116, 20303–20308.
- (22) Lampkin, B. J.; Nguyen, Y. H.; Karadakov, P. B.; VanVeller, B. Demonstration of Baird's rule complementarity in the singlet state with implications for excited-state intramolecular proton transfer. *Phys. Chem. Chem. Phys.* **2019**, 21, 11608–11614.
- (23) Ottosson, H. Exciting excited-state aromaticity. *Nat. Chem.* **2012**, 4, 969–971.
- (24) Rosenberg, M.; Dahlstrand, C.; Kilså, K.; Ottosson, H. Excited state aromaticity and antiaromaticity: opportunities for photophysical and photochemical rationalizations. *Chem. Rev.* **2014**, 114, 5379–5425.
- (25) Papadakis, R.; Ottosson, H. The excited state antiaromaticity benzene ring: a molecular Mr Hyde? *Chem. Soc. Rev.* **2015**, 44, 6472–6493.
- (26) Slanina, T.; Ayub, R.; Toldo, J.; Sundell, J.; Rabten, W.; Nicaso, M.; Alabugin, I.; Galván, I. F.; Gupta, A. K.; Lindh, R.; Orthaber, A.; Lewis, R. J.; Grönberg, G.; Bergman, J.; Ottosson, H. Impact of excited-state antiaromaticity relief in a fundamental benzene photoreaction leading to substituted bicyclo[3.1.0]hexenes. *J. Am. Chem. Soc.* **2020**, 142, 10942–10954.
- (27) Corminboeuf, C.; Heine, T.; Seifert, G.; Schleyer, P. v. R. Induced magnetic field in aromatic [n]-annulenes—interpretation of NICS tensor components. *Phys. Chem. Chem. Phys.* **2004**, 6, 273–276.
- (28) Chen, Z.; Wannere, C. S.; Corminboeuf, C.; Puchta, R.; Schleyer, P. v. R. Nucleus-independent chemical shifts (NICS) as an aromaticity criterion. *Chem. Rev.* **2005**, 105, 3842–3888.
- (29) Gogonea, V.; Schleyer, P. v. R.; Schreiner, P. R. Consequences of triplet aromaticity in $4n\pi$ -electron annulenes: calculation of magnetic shieldings for open-shell species. *Angew. Chem. Int. Ed.* **1998**, 37, 1945–1948.
- (30) Zhu, J.; An, K.; Schleyer, P. v. R. Evaluation of triplet aromaticity by the isomerization stabilization energy. *Org. Lett.* **2013**, 15, 2442–2445.
- (31) Werner, H.-J.; Knowles, P. J.; Knizia, G.; Manby, F. R.; Schütz, M. Molpro: a general-purpose quantum chemistry program. *WIREs Comput. Mol. Sci.* **2012**, 2, 242–245.
- (32) Aidas, K.; Angeli, C.; Bak, K. L.; Bakken, V.; Bast, R.; Boman, L.; Christiansen, O.; Cimiraglia, R.; Coriani, S.; Dahle, P.; Dalskov, E. K.; Ekström, U.; Enevoldsen, T.; Eriksen, J. J.; Ettenhuber, P.; Fernández, B.; Ferrighi, L.; Fliegl, H.; Frediani, L.; Hald, K.; Halkier, A.; Hättig, C.; Heiberg, H.; Helgaker, T.; Hennum, A. C.; Hetttema, H.; Hjertnæs, E.; Høst, S.; Høyvik, I.-M.; Iozzi, M. F.; Jansik, B.; Jensen, H. J. A.; Jonsson, D.; Jørgensen, P.; Kauczor, J.; Kirpekar, S.; Kjergaard, T.; Klopper, W.; Knecht, S.; Kobayashi, R.; Koch, H.; Kongsted, J.; Krapp, A.; Kristensen, K.; Ligabue, A.; Lutnæs, O. B.; Melo, J. I.; Mikkelsen, K. V.; Myhre, R. H.; Neiss, C.; Nielsen, C. B.; Norman, P.; Olsen, J.; Olsen, J. M. H.; Osted, A.; Packer, M. J.; Pawłowski, F.; Pedersen, T. B.; Provasi, P. F.; Reine, S.; Rinkevicius, Z.; Ruden, T. A.; Ruud, K.; Rybkin, V. V.; Salek, P.; Samson, C. C. M.; de Merás, A. S.; Saue, T.; Sauer, S. P. A.; Schimmelpfennig, B.; Sneskov, K.; Steindal, A. H.; Sylvester-Hvid, K. O.; Taylor, P. R.; Teale, A. M.; Tellgren, E. I.; Tew, D. P.; Thorvaldsen, A. J.; Thøgersen, L.; Vahtras, O.; Watson, M. A.; Wilson, D. J. D.; Ziolkowski, M.; Ågren, H. The Dalton quantum chemistry program system. *WIREs Comput. Mol. Sci.* **2013**, 4, 269–284.
- (33) Dalton, a molecular electronic structure program, Release v2016.2 (2017), see <http://daltonprogram.org>
- (34) Fliegl, H.; Taubert, S.; Lehtonen, O.; Sundholm, D. The gauge including magnetically induced current method. *Phys. Chem. Chem. Phys.* **2011**, 13, 20500–20518.
- (35) Krygowski, T. M. Crystallographic studies of inter- and intramolecular interactions reflected in aromatic character of π -electron systems. *J. Chem. Inf. Comput. Sci.* **1993**, 33, 70–78.
- (36) Aihara, J.-I. Aromaticity-based theory of pericyclic reactions. *Bull. Chem. Soc. Jpn.* **1978**, 51, 1788–1792.
- (37) Karadakov, P. B. Ground- and excited-state aromaticity and antiaromaticity in benzene and cyclobutadiene. *J. Phys. Chem. A* **2008**, 112, 7303–7309.
- (38) Karadakov, P. B. Aromaticity and antiaromaticity in the low-lying electronic states of cyclooctatetraene. *J. Phys. Chem. A* **2008**, 112, 12707–12713.
- (39) Karadakov, P. B.; Hearnshaw, P.; Horner, K. E. Magnetic shielding, aromaticity, and bonding in the low-lying electronic states of benzene and cyclobutadiene. *J. Org. Chem.* **2016**, 81, 11346–11352.
- (40) Turro, N. J.; Ramamurthy, V.; Scaiano, J. C. Modern molecular photochemistry of organic molecules. University Science Books: Sausalito, CA. **2010**, 1084pp.

- (41) Fries rearrangement. http://en.wikipedia.org/wiki/Fries_rearrangement, accessed March 22, 2021.
- (42) Reimers, J. R.; Cai, Z.-L. Hydrogen bonding and reactivity of water to azines in their S_1 (n,π^*) electronic excited states in the gas phase and in solution. *Phys. Chem. Chem. Phys.* **2012**, *14*, 8791–8802.
- (43) Liu, X.; Sobolewski, A. L.; Borrelli, R.; Domcke, W. Computational investigation of the photoinduced homolytic dissociation of water in the pyridine-water complex. *Phys. Chem. Chem. Phys.* **2013**, *15*, 5957–5966.
- (44) Liu, X.; Sobolewski, A. L.; Domcke, W. Photoinduced oxidation of water in the pyridine-water complex: comparison of the singlet and triplet photochemistries. *J. Phys. Chem. A* **2014**, *118*, 7788–7795.
- (45) Esteves-López, N.; Coussan, S.; Dedonder-Lardeux, C.; Jouvet, C. Photoinduced water splitting in pyridine water clusters. *Phys. Chem. Chem. Phys.* **2016**, *18*, 25637–25644.
- (46) Pang, X.; Jiang, C.; Xie, W.; Domcke, W. Photoinduced electron-driven proton transfer from water of an N-heterocyclic chromophore: nonadiabatic dynamics studies for pyridine–water clusters. *Phys. Chem. Chem. Phys.* **2019**, *21*, 14073–14079.
- (47) Maksyutenko, P.; Rizzo, T. R.; Boyarkin, O. V. A direct measurement of the dissociation energy of water. *J. Chem. Phys.* **2006**, *125*, 181101.
- (48) Romero, N. A.; Margrey, K. A.; Tay, N. E.; Nicewicz, D. A. Site-selective arene C–H amination via photoredox catalysis. *Science*, **2015**, *249*, 1326–1330.
- (49) Liu, X.; Karsili, T. N. V.; Sobolewski, A. L.; Domcke, W. Photocatalytic water splitting with the acridine chromophore: a computational study. *J. Phys. Chem. B* **2015**, *119*, 10664–10672.
- (50) McManus, J. B.; Nicewicz, D. A. Direct C–H cyanation of arenes via organic photoredox catalysis. *J. Am. Chem. Soc.* **2017**, *139*, 2880–2883.
- (51) Tay, N. E. S.; Nicewicz, D. A. Cation radical accelerated nucleophilic aromatic substitution via organic photoredox catalysis. *J. Am. Chem. Soc.* **2017**, *139*, 16100–16104.
- (52) Dang, H. T.; Haug, G. C.; Nguyen, V. T.; Vuong, N. T. H.; Nguyen, V. D.; Arman, H. D.; Larionov, O. V. Acridine photocatalysis: insights into the mechanism and development of a dual-catalytic direct decarboxylative conjugate addition. *ACS Catal.* **2020**, *10*, 11448–11457.
- (53) Nguyen, V. T.; Nguyen, V. D.; Haug, G. C.; Vuong, N. T. H.; Dang, H. T.; Arman, H. D.; Larionov, O. V. Visible-light-enabled direct decarboxylative N-alkylation. *Angew. Chem. Int. Ed.* **2020**, *59*, 7921–7927.